


One-Way Acoustic Guiding Under Transverse Fluid Flow

Ohad Silbiger¹ and Yakir Hadad^{1*}

School of Electrical Engineering, Tel-Aviv University, Ramat-Aviv, Tel-Aviv 69978, Israel

 (Received 15 February 2021; revised 4 May 2022; accepted 12 May 2022; published 29 June 2022)

In a moving acoustic medium, sound waves travel differently with and against the fluid flow. This well-established acoustic effect is backed by the intuition that the fluid velocity bias imparts momentum on the propagating acoustic waves, thus violating reciprocity. Based on this conception, fluid flow that is transverse to the wave direction of propagation will not break reciprocity. In this paper we contrast this common wisdom and theoretically show that the interplay between transverse mean flow and transverse structural gliding asymmetry can yield strong nonreciprocity and even, surprisingly, one-way acoustic waveguiding. To demonstrate that, we analyze a waveguide that comprises a few adjacent acoustic subdiffraction chains, i.e., linear chains of acoustic scatterers with monopolar or dipolar response. The structure is embedded within a medium with mean flow velocity that is *transverse to the waveguide axis*. We find the symmetry breaking conditions under which nonreciprocity is obtained, and we show how, under transverse mean flow, with Mach numbers as low as 0.02, one-way propagation of the acoustic wave is obtained on a sub-wavelength-thick acoustic waveguide. To demonstrate the phenomenon, we introduce two models. One in which the scatterers are assumed to be pointlike and the flow is homogeneous, and a second, in which we accommodate the issue of possible wakes created by the presence of scatterers inside the flow. The latter setup exhibits no direct interaction of the scatterers with the flow, by placing the waveguide in a quiescent medium adjacent to a flowing medium. Our results push forward the understanding of acoustic nonreciprocity, and may open another venue for the design of nonreciprocal acoustic wave devices for various applications.

DOI: [10.1103/PhysRevApplied.17.064058](https://doi.org/10.1103/PhysRevApplied.17.064058)

I. INTRODUCTION

Acoustic nonreciprocity has gained a lot of attention in recent years due to its numerous potential applications [1,2]. It can be achieved using nonlinearities [3–5], and by using active elements [6–8], but nevertheless, nonreciprocal acoustic propagation is mostly known to occur in moving media [9–12]. To illustrate that, assume that two friends, Alfred and Beth, shown in Fig. 1(a), are located at points A and B on the x axis, the distance between them is L , and that they communicate via plane waves that travel along the x axis in a fluid with uniform mean flow velocity $U_0\hat{x}$, and acoustic wave speed c . Using simple kinematic arguments, the time it takes for a signal from Alfred to reach Beth is different than the time it takes for a signal to propagate in the reciprocal direction,

$$\tau_d^{A\leftrightarrow B} = \frac{L}{c \pm U_0}. \quad (1)$$

Clearly, in light of Eq. (1), nonreciprocity that is caused due to a collinear fluid flow is rather weak at low Mach numbers, $q_0 = U_0/c \ll 1$. Nevertheless, in the presence of

sharp resonances the effect may be enhanced, giving rise even to isolation. This has been demonstrated, for example, using resonant cavities [13–16], waveguides connected in a sensitive Mach-Zehnder interferometer setup [17], and near zero index metamaterial waveguides [18]. Moreover, faster *synthetic* motion and thereby stronger nonreciprocity, may be emulated by space-time-modulated acoustic metamaterials [19–24]. In contrast, if, as illustrated in Fig. 1(b), the fluid flows *transverse* to the direction of propagation, that is, if, for instance, Alfred and Beth are located on the x axis as before, but the fluid flow velocity is $U_0\hat{z}$, the time delay for a plane wave to propagate between them is

$$\tau_d^{A\leftrightarrow B} = \frac{L}{c}, \quad (2)$$

as in a stationary fluid [25]. The exact results in Eqs. (1) and (2) are highly intuitive from the kinematic point of view, which implies, allegedly, that in the presence of a uniform mean flow, the communication between Alfred and Beth will be nonreciprocal only if the wave that propagates between them has some wavevector component that is parallel to the fluid stream.

*hadady@eng.tau.ac.il

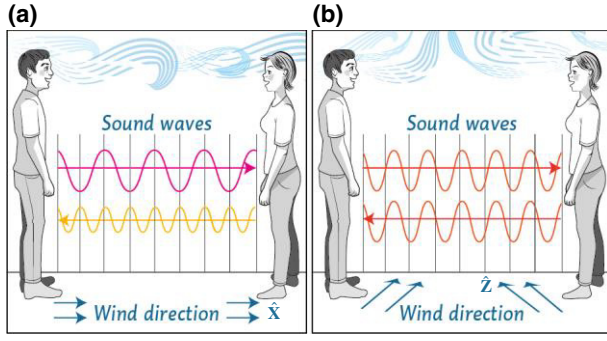


FIG. 1. (a) If the medium between Alfred and Beth is flowing in the same direction as the waves that propagate between them, different wave behavior is expected when the propagation is from left to right or vice versa. (b) If the medium between Alfred and Beth is flowing transversely to the waves that propagate between them, the waves are expected to propagate reciprocally.

In contrast with this common wisdom, in this paper we show that, under certain conditions, it is also possible to achieve strong nonreciprocity for waves that are propagating along a direction that is *transverse* to the mean flow velocity of the ambient medium. As we show below, this is achieved by the *near field* interplay between the transverse flow and structural transverse gliding asymmetry. Remarkably, in this way we demonstrate below *one-way guiding* with low Mach number flow and along a sub-wavelength-thick waveguide. Under these conditions, Alfred will be heard by Beth, while Beth will not be heard by Alfred, or vice versa, although the flow is transverse to the communication channel between them.

II. LINEAR CHAINS OF POINT SCATTERERS INSIDE UNIFORM FLOW

A. Description of the model

We consider a waveguide that comprises N periodic linear chains of acoustic scatterers that are surrounded by a medium with uniform *transverse* flow with respect to the waveguide axis. All the scatterers are assumed to be point-like and thus with low Reynolds number, introducing no wakes in the uniform flow. Later in Sec. III this assumption will be lifted. All the chains are located on the $y = 0$ plane, parallel to the x axis, and consist of a periodic arrangement of scatterers (modeled by their acoustic susceptibilities as point sources) that are equally spaced with acoustically small interscatterer spacing $d < \lambda/2$ [26], where λ is the acoustic wavelength. See the illustration in Fig. 2 with $N = 3$. The n th scatterer of chain number i ($i = 1, \dots, N$) is located at $\mathbf{r}_n^i = (d_x^i + nd, 0, d_z^i)$. Here, d_z^i denotes the z coordinate of the i th chain, where $d_z^1 = 0$ so that the first chain is located right on the x axis. And, d_x^i is the *gliding* distance of the i th chain with respect to the origin. For the first ($i = 1$) chain, $d_x^1 = 0$. Thus, the spacing between

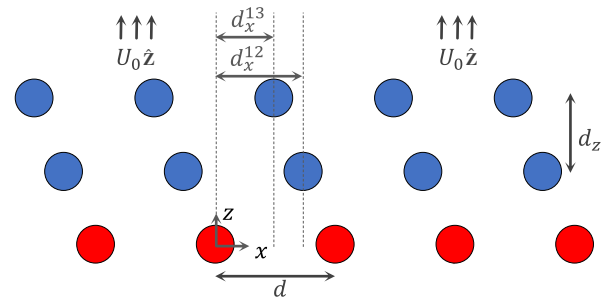


FIG. 2. A periodic waveguide structure with transverse asymmetry. As an example, we consider one chain of monopoles and two chains of longitudinal dipoles. The entire structure is embedded in a medium with mean transverse flow. Here d is the interscatterer spacing along each one of the chains, and $d_z = 0.33d$ is the distance between chains. The lattice gliding asymmetry is determined by the chain gliding parameters that in this example are $d_x^{12} = 0.66d$ and $d_x^{13} = 0.5d$.

the chains i and j is given by $d_z^{ij} = d_z^j - d_z^i$, and the relative gliding between them reads $d_x^{ij} = d_x^j - d_x^i$. The entire structure is surrounded by a medium with a uniform mean flow velocity $\mathbf{U}_0 = U_0 \hat{z}$ that is transverse to the waveguide axis x .

The acoustic scatterers are modeled as point sources, and therefore all interactions between the scatterers and the flow are neglected. We assume that the scatterers exhibit either a dominant monopole or dipole response. For example, in Fig. 2, chain $i = 1$ consists of monopole scatterers while chains $i = 2, 3$ consist of dipole scatterers with a response that is polarized along the x axis. The scatterers are characterized by their acoustic susceptibilities, α^{mm} and α_ξ^{dd} , which link the local field, i.e., the field in the scatterer's location but in the absence of the scatterer itself, to the resulting scattering response. Specifically, the monopole is characterized by a volume V (in units of m^3) and is induced by a local pressure P , while the dipole is characterized by a dipole moment D_ξ (in units of m^4) and is induced by the space derivative of the local pressure in the direction $\xi = x, y, z$. Thus,

$$V = \alpha^{mm} P, \quad D_\xi = \alpha_\xi^{dd} \frac{\partial P}{\partial \xi}. \quad (3)$$

Note that in a quiescent medium ($U_0 = 0$) the induced dipole moment is proportional to the pressure gradient that is proportional to the particle velocity. The latter is not true in a medium with mean fluid flow [12]. The dipole is excited by the pressure gradient, and, therefore, we associate directly the induced dipole moment with the pressure spatial derivative.

Once the induced source on the scatterer is known, the scattered field generated by the scatterer is given via the corresponding Green's function. To derive this relationship mathematically, we consider a time-harmonic monopole

source with volume V located at the origin and surrounded by a medium with wave velocity c_0 , and a uniform mean flow velocity $\mathbf{U}_0 = U_0 \hat{z}$. The velocity potential of the source reads [12]

$$\Psi_m(\rho, z) = j \omega V \frac{e^{-jk\sqrt{q^2\rho^2+z^2}/q^2}}{4\pi\sqrt{q^2\rho^2+z^2}} e^{j(kq_0z/q^2+\omega t)}, \quad (4)$$

where $\rho^2 = x^2 + y^2$, $k = \omega/c_0$ is the wave number in stationary medium, $q_0 = U_0/c_0$ is the flow Mach number, and $q^2 = 1 - q_0^2$. The pressure field is given by

$$P = j \omega \rho_0 \Psi_m + U_0 \rho_0 \frac{\partial \Psi_m}{\partial z}, \quad (5)$$

where ρ_0 is the medium density. For the dipoles, we use the fact that the pressure generated by the dipole is the spatial derivative of the pressure generated by the monopole, with respect to the coordinate along which the dipole is polarized (see Appendix A). Thus, we use the function Ψ_m and its derivatives to obtain the relationship between the source terms (V , D_x , and D_z) and the resulting acoustic fields. This is compactly formulated into a dyadic Green's function as

$$\begin{pmatrix} P \\ \partial_x P \\ \partial_z P \end{pmatrix} = \begin{pmatrix} G^{mm} & G_x^{dm} & G_z^{dm} \\ G_x^{md} & G^{dd} & G_{zx}^{dd} \\ G_z^{md} & G_{xz}^{dd} & G^{dd} \end{pmatrix} \begin{pmatrix} V \\ D_x \\ D_z \end{pmatrix}, \quad (6)$$

where $\partial_x P = \partial P / \partial x$, $\partial_z P = \partial P / \partial z$, and the first and second superscripts (d for dipole and m for monopolar) of the terms in G denote the source and excited scatterer types, respectively. We use this notation because later on it will be of interest to calculate the local fields in the waveguide, where monopoles and dipoles affect each other. Also, these functions will be used to construct mathematical expressions for the effect of the waveguide chains on each other. For full analytical expressions of Green's functions, see Appendix A.

The acoustic scatterers are assumed to be passive and lossless; therefore, the susceptibilities, α^{mm} and α_ξ^{dd} in Eq. (3), are subject to energy conservation. This implies for example that, for α^{mm} , given a local pressure field P that induces a monopole source with acoustic volume V , the power invested by the field for the scatterer excitation, $-(\omega/2)\text{Im}(V^*P)$, has to be equal to the power radiated by the scatterer, $(\omega^3 k \rho_0 / 8\pi q^4) |V|^2$. Thus, an energy conserving scatterer with monopolar response will be represented by α^{mm} that satisfies

$$\text{Im}\left(\frac{1}{\alpha_{mm}}\right) = -\frac{\omega^3 \rho_0}{4\pi q^4 c_0}. \quad (7)$$

This relation is known as the *radiation correction* of the scatterer's susceptibility, here, for a scatterer in a moving fluid. Similarly, for the longitudinal x dipole and the

transverse z dipole,

$$\text{Im}\left(\frac{1}{\alpha_x^{dd}}\right) = -\frac{\omega^5 \rho_0}{12\pi q^6 c_0^3}, \quad (8)$$

$$\text{Im}\left(\frac{1}{\alpha_z^{dd}}\right) = -\frac{\omega^5 \rho_0}{12\pi q^8 c_0^3} (1 + 5q_0^2). \quad (9)$$

A full derivation of the radiation correction can be found in Appendix B. Note that the fluid flow has to be taken into account precisely in the calculation of this radiation correction in order to properly find the dispersion relation of the propagating modes on the lattice. As opposed to the imaginary part of the inverse of the susceptibilities, which, for lossless scatterers, is independent of the scatterer's geometry and material, the real parts $\text{Re}(1/\alpha^{mm})$ and $\text{Re}(1/\alpha_\xi^{dd})$ depend on the particular scatterer's characteristics. Such a scatterer may for instance be a Helmholtz resonator [12] or some variation over it [27]. In our simulations, the susceptibility values are characterized as a Lorentzian function of frequency:

$$\frac{1}{\alpha} = A(\omega^2 - \omega_r^2) + j \text{Im}\left(\frac{1}{\alpha}\right). \quad (10)$$

Here ω_r is the resonance frequency, A is an amplitude constant, and the imaginary part is selected to satisfy the radiation correction of the source type (V , D_x , and D_z) as per Eqs. (7)–(9). Selected parameters for the proposed waveguide are

$$A = 10, \quad \omega_r = 7070 \text{ rad/s} \quad (\text{monopole parameters}),$$

$$A = 0.001, \quad \omega_r = 21\,210 \text{ rad/s} \quad (\text{dipole parameters}).$$

The waveguide behavior is simulated around the frequency $f_0 = 1125$ Hz ($\omega_0 = 7070$ rad/s). The parameter selection above generates a resonant behavior of the monopoles at $\omega = \omega_0$, while the dipoles show no resonance around this frequency. Susceptibility plots are shown in Fig. 3.

B. Guided modes

Since the lattice is infinite, we assume that the induced sources on the scatterers behave in a Bloch form, i.e., exhibiting a wave behavior

$$X_n^i = X_0^i e^{-j\beta n d}, \quad (11)$$

where β is an unknown complex constant. Henceforth, we use X_n^i to denote the moment of scatterer n in chain i , which may be a monopole (V) or a dipole (D_x or D_z). Given a specified spatial configuration of the waveguide, such as in Fig. 2, our interest is to find the guided modes that may propagate through it, and are characterized by the propagation constant β .

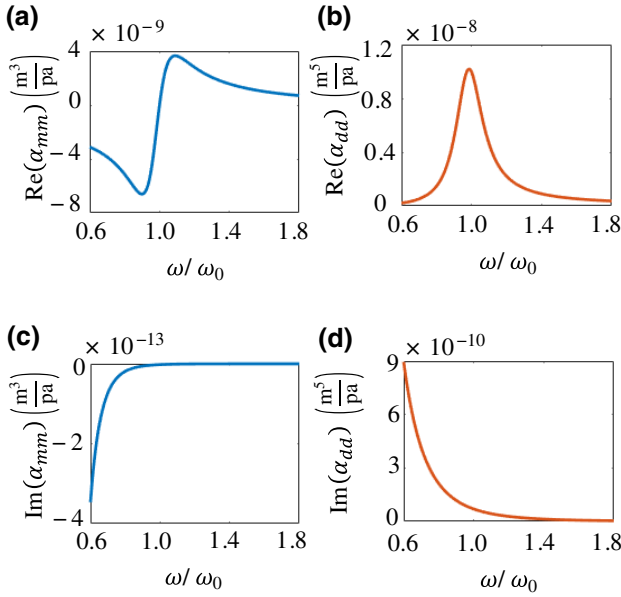


FIG. 3. Monopole and dipole susceptibility functions used in the numerical simulations.

Given two scatterers, X_1 and X_2 , that are located at \mathbf{r}_1 and \mathbf{r}_2 in a homogeneous medium with mean flow velocity $U_0\hat{\mathbf{z}}$, we denote by G^{12} the Green's function that relates the source X_1 to the field that excites X_2 . For example, if the scatterers are both monopoles then $X_1 = V_1, X_2 = V_2$, and G^{12} is defined such that $P(\mathbf{r}_2) = G^{12}(\mathbf{r}_2 - \mathbf{r}_1)V_1$. Thus, for two chains with indices i and j , we define their mutual Green's function S^{ij} as the local field at X_0^j , caused by chain i :

$$S^{ij}(\beta) = \sum_{n=-\infty}^{\infty} G^{ij}(d_x^{ij} - nd, d_z^{ij})e^{-j\beta nd}, \quad (12)$$

$$S^{ii}(\beta) = \sum_{n \neq 0} G^{ii}(-nd, 0)e^{-j\beta nd}. \quad (13)$$

To calculate the series in Eqs. (12) and (13), we have used common summation techniques, leading to polylogarithms (for S^{ii}) and using Poisson summation (for S^{ij}). A full derivation can be found in Appendices C and D. Thus, the modal dynamics of a waveguide with N parallel chains is governed by the linear system

$$\begin{bmatrix} \alpha^1 & 0 & \dots \\ \vdots & \ddots & \\ 0 & & \alpha^N \end{bmatrix} \begin{bmatrix} S^{11} & S^{12} & \dots \\ \vdots & \ddots & \\ S^{N1} & & S^{NN} \end{bmatrix} \begin{bmatrix} X_0^1 \\ \vdots \\ X_0^N \end{bmatrix} = \begin{bmatrix} X_0^1 \\ \vdots \\ X_0^N \end{bmatrix}, \quad (14)$$

where α^i is the susceptibility of the scatterers that comprise chain i . The waveguide modes are nontrivial solutions of homogeneous system (14) and, as such, satisfy the

dispersion relation

$$\det[\underline{\underline{\alpha}}(\omega)^{-1} - \underline{\underline{S}}(\omega, \beta)] = 0. \quad (15)$$

Nontrivial real β solutions will exist only if $d < \lambda/2$ [26], implying sub-wavelength-mode width, as expected by a subdiffraction waveguide (see Refs. [28–30] for reciprocal and nonreciprocal similar waveguides in optics). Importantly, as shown in the following, the properties of $\underline{\underline{S}}$ are affected by the transverse mean flow $\mathbf{U}_0 = U_0\hat{\mathbf{z}}$ and hence determine the structure's reciprocity and even enable one-way guiding along the x axis.

In a reciprocal waveguide, for each frequency, propagation is allowed in both directions with equal phase and group velocities. Therefore, in such a waveguide, for each frequency, if β is a solution to Eq. (15), so is $-\beta$. As will be shown, under certain conditions, the transverse mean flow yields nonreciprocal propagation along the waveguide axis. This nonreciprocal behavior is manifested in the properties of $\underline{\underline{S}}$. If $q_0 = 0$, reciprocity of the waveguide is expected. In this case, the symmetry (or antisymmetry) of all Green's functions G^{ij} with respect to x and z leads readily to the conclusion that $\underline{\underline{S}}(-\beta) = \underline{\underline{S}}^T(\beta)$, and therefore, for any given frequency ω , if β solves Eq. (15), so does $-\beta$. See Appendix E for a full proof. Moreover, if the waveguide contains zero or half-step gliding for any number of chains, i.e., if, for all $i \neq j$, $d_x^{ij} = 0$ or $d_x^{ij} = d/2$, the waveguide is symmetric for propagation towards the positive or negative x axis. In this case spatial symmetry also imposes reciprocity when transverse flow is present. It requires transverse flow *and* spatial asymmetry in the form of gliding to breach reciprocity. This longitudinal nonreciprocity originates from the interplay between transverse gliding asymmetry and the transverse nonreciprocal interaction between the scatterers due to the mean flow. Lastly, it should be emphasized that if the chains are distant from each other ($d_z \gg d$), the off-diagonal terms of $\underline{\underline{S}}$ are negligible relative to the diagonal terms, thus making the waveguide negligibly nonreciprocal. This implies that this nonreciprocal behavior cannot be explained using kinematic arguments that are applied on plane waves or that may be applied on local plane waves propagating along ray trajectories between adjacent scatterers (see Sec. IV for a kinematic analysis). Instead, the transverse microscale dynamics of the mode plays an important role in this strong nonreciprocal effect.

C. One-way guiding

In any case when the waveguide is introduced with transverse flow as well as transverse gliding asymmetry, it will be nonreciprocal. However, this behavior is not always strong enough to be observed, especially in low flow speeds. To maximize this nonreciprocal effect, the structure in Fig. 2 is purposed. The structure consists of a

chain of monopoles and two chains of longitudinal dipoles, while asymmetry is introduced by shifting the middle chain by $0.66d$. The medium is air with $c_0 = 343$ m/s and $\rho_0 = 1.2$ kg/m³. The monopoles are resonant around the frequency $f_0 = 1125$ Hz, while the dipoles exhibit no resonance around this frequency (see Fig. 3). By solving Eq. (15) numerically we find the dispersion relation $\omega(\beta)$ that is plotted in Fig. 4 for a number of cases. In the absence of medium flow and when the structure is transversely symmetric, the dispersion relation is symmetric in β , as shown in Fig. 4(a), and the waveguide is reciprocal. Reciprocity and thereby symmetric dispersion is also maintained for $d_x^{12} = 0$ or $d/2$ and $d_x^{13} = 0$ or $d/2$ but $q_0 \neq 0$ [as an example, see Fig. 4(b)] and for $d_x^{12}, d_x^{13} \neq 0$ or $d/2$ but $q_0 = 0$ [as an example, see Fig. 4(c)]. However, as soon as transverse flow is introduced simultaneously with a transversely gliding asymmetric structure, $d_x^{12}, d_x^{13} \neq 0$ or $d/2$ and $q_0 \neq 0$, then reciprocity in the longitudinal direction is broken and the dispersion relation becomes asymmetric, as shown in Fig. 4(d). In the latter case, for the gliding parameters, we used $d_x^{12} = 0.66d$ and

$d_x^{13} = 0.5d$, and spacing $d_z = 0.33d$, where the interscatterer spacing is given by $d = 0.1\lambda_0$ with $\lambda_0 = c_0/f_0$. For the proposed structure, observable nonreciprocity can be obtained in Mach numbers as low as $q_0 \sim 0.02$, as shown in Fig. 4(d). With a moderate Mach number, $q_0 = 0.1$, by the dispersion diagram we see that, remarkably, the waveguide allows propagation only in the positive direction of the x axis as only positive group velocity is present. As the flow velocity becomes larger, so does the one-way bandwidth, as evident by comparing the dispersion diagrams for the $q_0 = 0.02$ and $q_0 = 0.1$ cases.

Physical manifestation of this one-way guiding can be observed in a chain of finite length. Given N chains of M scatterers each, the local field at each scatterer is defined via summation of the external field contributions of all neighboring scatterers. The amplitude of X_n^j satisfies

$$X_n^j = \alpha^j P_0(\mathbf{r}_n^j) + \alpha^j \sum_{i=1}^N \sum_{m=1}^M G^{ij} [d_x^{ij} + (m-n)d, d_z^{ij}] X_m^i, \quad (16)$$

where P_0 is the external field that excites the scatterer and G^{ij} is Green's function that relates the source X_m^i to the field that excites X_n^j . Formulating this equation for every scatterer, we obtain a system of MN equations with MN unknowns. To formulate this in matrix form, we represent the scatterer amplitudes in the waveguide as a vector \mathbf{X} of size $[MN \times 1]$, so that elements $1, \dots, N$ correspond to the scatterers in chain 1, elements $N+1, \dots, 2N$ correspond to the scatterers in chain 2, and so on. Thus, X_m^i is mapped to $\mathbf{X}[(i-1)N + m]$. Then, from Eq. (16), \mathbf{X} should satisfy

$$[\underline{\alpha}^{-1} - \underline{G}]\mathbf{X} = \mathbf{P}_0, \quad (17)$$

where \mathbf{P}_0 is the vector of the external field acting on each scatterer, corresponding to \mathbf{X} , and the matrix \underline{G} represents the mutual effect of the scatterers through the free-space proper Green's function.

To demonstrate one-way guiding, a finite chain is excited by applying a localized external pressure field on a monopole scatterer in the middle of chain $i = 1$. Then, the resulting excitation amplitudes of all the scatterers are solved numerically via matrix inversion. The result of such a calculation is shown in Fig. 5 for a waveguide with 400 unit cells. The lattice parameters used here are those that were used to calculate Fig. 4(d), with Mach number $q_0 = 0.1$ and at frequency $\omega = 1.4\omega_0$ [marked in Fig. 4(d)]. This result nicely demonstrates how, under transverse mean flow, with low Mach number, longitudinal one-way rightward propagation of the acoustic wave is obtained, while leftward propagation is practically prohibited. Instead, rapid exponential decay takes place in the forbidden direction, indicating that a complex leaky mode is excited in this direction. Furthermore, the plateau level

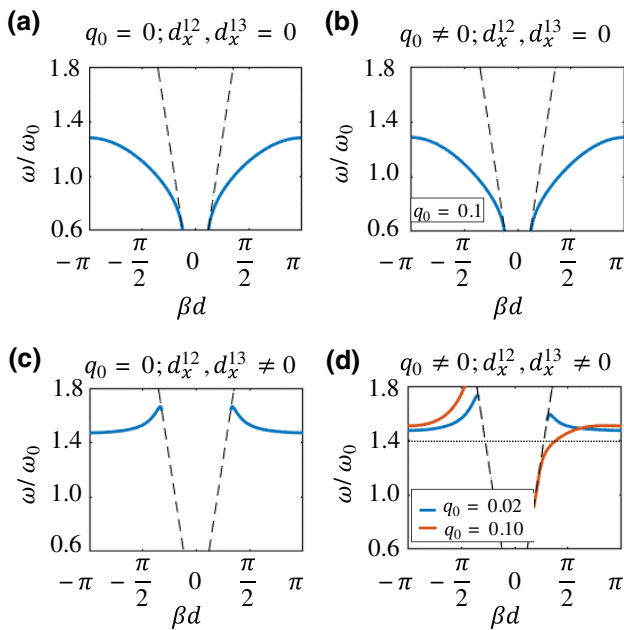


FIG. 4. Dispersion plots for a waveguide comprised three scatterer chains; see Fig. 2. (a) In a quiescent medium with no chain gliding, the propagating mode is symmetric, i.e., both solutions have equal phase and group velocities, but in opposite directions. (b) Adding transverse flow while maintaining zero gliding changes the dispersion plots very slightly, without affecting the reciprocal nature of the waveguide. (c) Introducing chain gliding in a quiescent medium changes the dispersion curves, but does not break reciprocity. (d) Combination of chain gliding asymmetry and transverse flow generates substantial nonreciprocity in the waveguide.

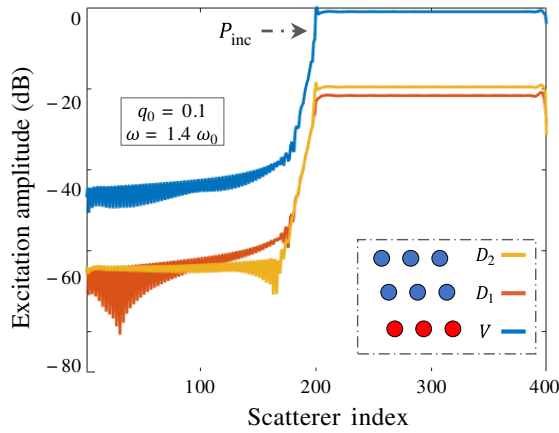


FIG. 5. Amplitudes of monopole and dipole strengths along a chain with 400 scatterers, due to a local external pressure field P_{inc} applied on a single monopole scatterer in the middle of chain $i = 1$. Only propagation to the right is allowed, consistent with the dispersion diagram predicted by the infinite chain model, as shown in Fig. 4(d).

that is reached beyond the fast decay is a consequence of a weakly excited continuous spectrum wave (also termed lateral wave) along the lattice. A detailed analysis of this excitation problem should follow Green’s function development for the waveguide under study here. Related work may be found in Hadad and Steinberg [31], and in Hadad *et al.* [32], who discuss the Green’s function of a plasmonic subdiffractive waveguide under magnetic biasing.

III. LINEAR CHAINS OF SCATTERERS INSIDE A STATIONARY MEDIUM DUCT WITH PERIPHERAL FLOW

A. Description of the model

In Sec. II we showed how a waveguide composed of point-source scatterers (monopoles and dipoles) can support nonreciprocal and even one-way guiding through a combination of transverse flow and transverse spatial asymmetry. However, physical implementation of such a waveguide should require the scatterers to be of finite size, thus obstructing the flow and maybe even changing the flow nature from laminar to turbulent at high enough Reynolds numbers. In the following, we suggest another scheme, under which there is no direct interaction between the scatterers and the flow. Using the same techniques, we reproduce the effects observed in the waveguide embedded in a medium with uniform flow, in a waveguide that is embedded in a stationary medium with peripheral flow.

Consider a waveguide similar to the waveguide presented before (see Fig. 2), located inside a duct with a quiescent (stationary) medium that is sandwiched between two half-spaces with uniform flow with velocity $U_0 \hat{z}$. We

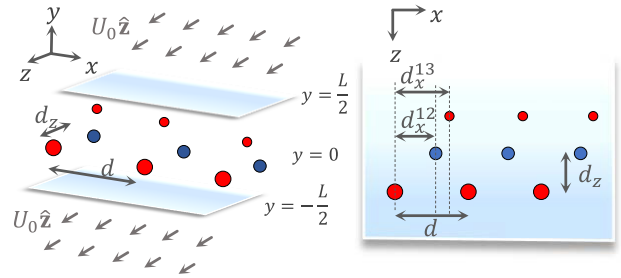


FIG. 6. A periodic waveguide with transverse asymmetry (left shows the side view, right shows the top view). As an example, the waveguide consists of three chains of acoustic scatterers, and is located in stationary fluid, between two half-spaces with mean transverse flow with velocity $U_0 \hat{z}$. Here d is the interscatterer spacing along each one of the chains, and d_z is the distance between chains. The lattice gliding asymmetry is determined by the chain gliding parameters, d_x^{12} and d_x^{13} . The waveguide is infinite in the x direction; three unit cells are shown.

assume that the density ρ_0 and the wave velocity c_0 are uniform in the entire space. Thus, the duct is created merely due to the inhomogeneous medium flow; see Fig. 6 for an illustration. This may be achieved using thin, acoustically transparent membranes placed at the interfaces, $y = -L/2$ and $y = L/2$. The boundary condition for this scheme has been extensively studied in, e.g., Ref. [33].

The equations governing the dynamics of the waveguide in the duct are exactly the same as those that govern the waveguide embedded in uniform flow. The dispersion relation in Eq. (15) is the same, and so is the calculation of the elements of \underline{S} , as per Eqs. (12) and (13). The only difference is the expression of the scatterers’ Green’s functions. These Green’s functions take into account the “direct” wave interaction between the scatterers, as well as the interaction by waves reflected from the boundaries with the uniform flow domains. Lastly, it should be noted that the radiation correction in this case uses $q_0 = 0$ [see Eqs. (7)–(9)], as the scatterers are surrounded by a stationary medium.

B. Green’s function—stationary medium between two half-spaces with uniform flow

Here we derive the analytical expression for the pressure field generated by an acoustic monopole scatterer in a stationary medium, sandwiched between two half-spaces with uniform flow. We start by introducing the reflection coefficient for a plane wave impinging on an interface between two media, each flowing with a different velocity, parallel to the interface. Then we represent the pressure field generated by the monopole as a spectrum of plane waves and calculate the spectrum of the field inside the duct as a summation of infinite plane-wave reflections. Lastly, we use

the inverse Fourier transform to calculate Green's function in space. The first two steps are calculated analytically, while the third and final step is evaluated numerically.

Assume two media with densities ρ_1, ρ_2 and sound speeds c_1, c_2 , flowing with mean velocities $\mathbf{U}_1 = U_1 \hat{\mathbf{z}}$ and $\mathbf{U}_2 = U_2 \hat{\mathbf{z}}$, respectively. Medium 1 fills the half-space $y < 0$ and medium 2 fills the half-space $y > 0$ [see Fig. 7(a)]. If a plane wave with angular frequency ω travels in medium 1 and impinges upon the boundary at $y = 0$, the boundary conditions that need to be satisfied on the interface at $y = 0$ will cause reflections, which will be nonsymmetric for waves coming from the positive or negative side of the z axis. The reflection coefficient from this boundary was presented in Ref. [33]. For an acoustic plane-wave field, the velocity potential in both media reads

$$\phi_1 = e^{j(k_x x + k_y y + k_z z)} + \text{Re} e^{j(k_x x - k_y y + k_z z)}, \quad (18)$$

$$\phi_2 = T e^{j(k_x x + k_y y + k_z z)}, \quad (19)$$

where

$$k_i = \frac{\omega - U_i k_z}{c_i}, \quad k_y^i = \sqrt{k_i^2 - k_x^2 - k_z^2}, \quad i = 1, 2. \quad (20)$$

The boundary conditions at $y = 0$ render

$$R = \frac{1 - A}{1 + A} \quad \text{and} \quad A = \frac{\rho_1 (c_1 k_1)^2 k_{y2}}{\rho_2 (c_2 k_2)^2 k_{y1}} \quad (21)$$

Now we consider the three-layer medium in Fig. 6. The middle layer, bounded between $y = -L/2$ and $y = L/2$, contains a stationary medium, with density ρ_0 and sound speed c_0 . At $y = -L/2$ and $y = L/2$ acoustically transparent membranes are placed. Above the top membrane and below the bottom membrane, a similar medium flows with velocity $\mathbf{U}_0 = U_0 \hat{\mathbf{z}}$. An acoustic monopole is placed at the origin. In this scheme, the acoustic field generated

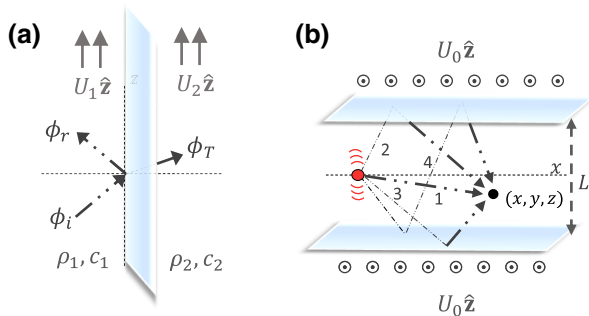


FIG. 7. (a) Reflection from a boundary between two flowing media. (b) The pressure field generated by a monopole source in a stationary medium, placed between two half-spaces with a flowing medium, is contributed to by (1) a “direct wave” and (2–4) an infinite number of reflected waves.

by the monopole can be treated as a superposition of two contributions—the field contributed directly by the source, without any reflections, and the field reflected from the boundaries—see Fig. 7(b). To calculate the field, we use the two-dimensional spectral decomposition of the wave generated by the monopole in free space:

$$g_{\text{FS}}^{mm}(y; k_x, k_z) = \frac{1}{4\pi^2} \iint_{-\infty}^{\infty} G_{\text{FS}}^{mm}(x, y, z) e^{j(k_x x + k_z z)} dx dz. \quad (22)$$

Here G_{FS}^{mm} is the monopole's Green's function in free space [12]:

$$G_{\text{FS}}^{mm}(x, y, z) = -\omega^2 \rho_0 \frac{e^{-jkr}}{4\pi r} \quad (23)$$

with $r = \sqrt{x^2 + y^2 + z^2}$ and $k = \omega/c_0$ the wave number in free space. Thus, the spectral decomposition reads

$$g_{\text{FS}}^{mm}(y; k_x, k_z) = j \omega^2 \rho_0 \frac{e^{-jk_y |y|}}{8\pi^2 k_y}, \quad (24)$$

where $k_y = \sqrt{k^2 - k_x^2 - k_z^2}$.

For the total field, we can consider four kinds of plane waves propagating from the monopole source to the observation point: (1) waves that propagate directly, without any reflections; (2) waves that experienced one reflection from the top boundary; (3) waves that experienced one reflection from the bottom boundary; and (4) waves that experienced two reflections [see Fig. 7(b)]. The mathematical representation of these waves' spectrum is

$$\frac{j \omega^2 \rho_0}{8\pi^2 k_y} [1 + \text{Re}^{-jk_y(L-y)} + \text{Re}^{-jk_y(L+y)} + R^2 e^{-jk_y(2L-|y|)}]. \quad (25)$$

To that we add the waves that experienced $2n$ more reflections— n reflections from each boundary, before reaching the observation point. Each such (double) reflection multiplies the amplitude of the wave by R^2 and adds a phase of $-2k_y L$. Also, the fields of interest are confined to the plane $y = 0$. Performing this substitution in Eq. (25) gives the total spectrum

$$g^{mm}(0; k_x, k_z) = \frac{j \omega^2 \rho_0}{8\pi^2 k_y} [1 + 2\text{Re}^{-jk_y L} + R^2 e^{-2jk_y L}] \times \sum_{n=0}^{\infty} (R^2 e^{-2jk_y L})^n, \quad (26)$$

which can be simplified to

$$g^{mm}(k_x, k_z) = \frac{j \omega^2 \rho_0}{8\pi^2 k_y} \frac{1 + \text{Re}^{-jk_y L}}{1 - \text{Re}^{-jk_y L}}. \quad (27)$$

Then we can apply the inverse transform to obtain the field

$$G^{mm}(x, z) = \iint_{-\infty}^{\infty} g^{mm}(k_x, k_z) e^{-j(k_x x + k_z z)} dk_x dk_z. \quad (28)$$

The integral in Eq. (28) should be calculated numerically. For practical reasons, it is easier to break the expression for the spectral Green's function given in Eq. (26) into two—one will consider the direct waves and the other will consider the reflected waves only. This is because adding the contribution of the direct waves into the numerical calculation causes convergence issues; however, it can be calculated very easily analytically. Therefore, we write

$$g^{mm}(0; k_x, k_z) = \frac{j\omega^2 \rho_0}{8\pi^2 k_y} \left[1 + \frac{2\text{Re}^{-jk_y L}}{1 - \text{Re}^{-jk_y L}} \right]. \quad (29)$$

The first element in Eq. (29) is the contribution of the direct waves. This element will be excluded from the numerical integration, and calculated from the free-space Green's function in Eq. (23). To summarize,

$$G^{mm}(x, z) = G_{\text{FS}}^{mm}(x, z) + G_r^{mm}(x, z), \quad (30)$$

where

$$G_{\text{FS}}^{mm}(x, z) = -\omega^2 \rho_0 \frac{e^{-jk\sqrt{x^2+z^2}}}{4\pi\sqrt{x^2+z^2}}, \quad (31)$$

$$G_r^{mm}(x, z) = \frac{j\omega^2 \rho_0}{8\pi^2} \iint_{-\infty}^{\infty} \frac{2\text{Re}^{-jk_y L}}{k_y(1 - \text{Re}^{-jk_y L})} \times e^{-j(k_x x + k_z z)} dk_x dk_z. \quad (32)$$

Expressions for the other Green's functions are obtained from G^{mm} through differentiation.

C. One-way guiding

Here we repeat the process of numerically solving Eq. (15) to find the dispersion relation $\omega(\beta)$, while using the Green's functions derived for the duct. For full expressions and derivations of the terms of the matrix \underline{S} , see Appendices F and G. The dispersion plots in Fig. 8 are an example of a waveguide in which this effect is strong to the extent that one-way guiding is obtained at low Mach numbers. In this case the structure consists of two chains of monopoles and three chains of longitudinal dipoles, shifted relative to one another to produce gliding asymmetry. The medium is air with $c_0 = 343$ m/s and $\rho_0 = 1.2$ kg/m³. The susceptibilities are the same as before; see Fig. 3. In the absence of medium flow ($q_0 = 0$) or when the structure is transversely symmetric (for all i, j , $d_x^j = 0$ or $d/2$), the dispersion relation is symmetric (in β), as shown in Figs. 8(a)–(c), and the waveguide is reciprocal. It is only when transverse flow is introduced simultaneously with a

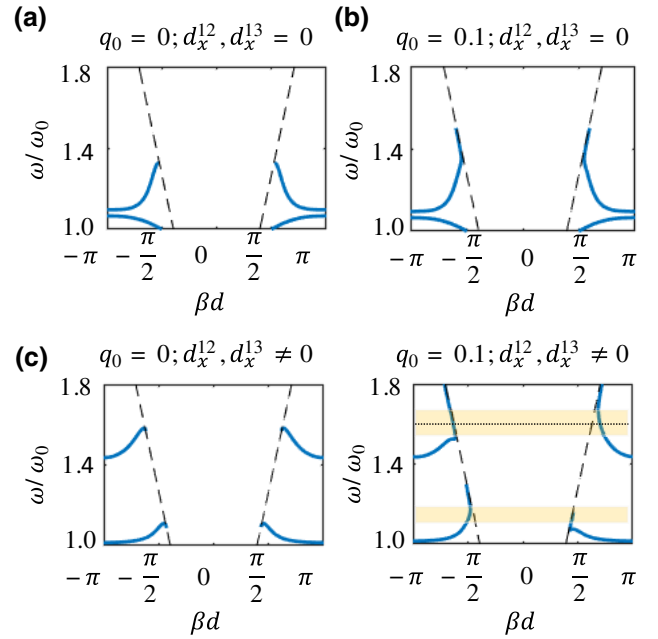


FIG. 8. Dispersion plots for a waveguide comprised five scatterer chains—two chains of monopoles and three chains of longitudinal dipoles. (a) With no flow above and below the duct and no chain gliding, the propagating mode is symmetric, i.e., both solutions have equal phase and group velocities, but in opposite directions. (b) Adding transverse flow while maintaining zero gliding changes the dispersion plots very slightly, without affecting the reciprocal nature of the waveguide. (c) Introducing chain gliding in a quiescent medium changes the dispersion curves, but does not break reciprocity. (d) Combination of chain gliding asymmetry and transverse flow generates substantial nonreciprocity in the waveguide.

transversely gliding-asymmetric structure that reciprocity in the longitudinal direction is broken and the dispersion relation becomes asymmetric, as shown in Fig. 8(d).

Again, we may formulate a finite excitation problem to demonstrate this nonreciprocal behavior. For a finite waveguide with M scatterers in each chain, we may formulate a system of equations as per Eq. (17), with $5M$ equations in this case. Figure 9 shows the excitation amplitudes along a waveguide with 400 unit cells upon excitation of a single monopole in the center of chain 1. The simulation is performed at excitation frequency $\omega = 1.6\omega_0$ [marked in Fig. 8(d)] and with $q_0 = 0.1$. As predicted by the dispersion plot, propagation of the wave to the left is allowed, while the wave decays exponentially in the right direction. Here we should note that the finite chain calculation adds numerical complexity, due to the integral in Eq. (32); see the elaboration in Appendix H.

IV. THE FAILURE OF KINEMATIC MODELS

In the previous sections we have shown that a coupled resonator waveguide that is placed in the vicinity

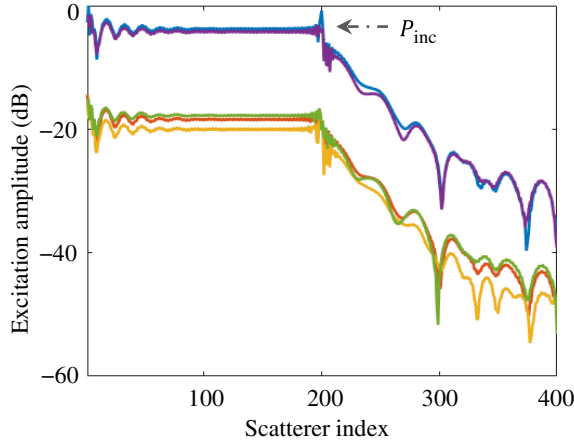


FIG. 9. Amplitudes of monopole and dipole strengths along a waveguide with five chains, 400 scatterers in each chain, due to a local external pressure field P_{inc} applied on a single monopole scatterer in the middle of chain $i = 1$. The blue line denotes V_n^1 , the orange line denotes D_{zn}^2 , the yellow line denotes D_{zn}^3 , the magenta line denotes V_n^4 , and the green line denotes D_{zn}^5 . The lattice parameters used are the same as in Fig. 8(d), with Mach number $q_0 = 0.1$ and at frequency $\omega = 1.6\omega_0$. Only propagation to the left is allowed, consistent with the negative group velocity obtained from the dispersion diagram in Fig. 8(d) at this frequency.

of a moving medium with flow velocity that is transverse with respect to the waveguide axis may become strongly nonreciprocal and even enable one-way propagation. These results cannot be predicted using mere kinematic arguments, and instead require to account for the field distribution. To show that, we consider here a kinematic coupled mode model that clearly fails to predict the main results of this paper. In such a model, the propagation may be considered as a hopping process between adjacent resonators.

Consider a coupled mode model for such a system. The coupling coefficients will be affected by the flow. Specifically, in the model shown in Fig. 10,

$$\kappa_{12} = |\kappa_{12}|e^{j\phi_{12}} = \kappa_{21}^*, \quad (33a)$$

$$\kappa_{23} = |\kappa_{23}|e^{j\phi_{23}} = \kappa_{32}^*, \quad (33b)$$

$$\kappa_{31} = |\kappa_{31}|e^{j\phi_{31}} = \kappa_{13}^*. \quad (33c)$$

Note that $\kappa_{12} = \kappa_{21}^*$ for energy conservation [34]. The magnitudes of the coupling coefficients are determined by the distance, orientation, and type of scatterers. Importantly, in this frequency domain representation, the phase term, for example, ϕ_{12} , corresponds to the difference in the “time of flight” of the acoustic wave that propagates between resonators 1 and 2. Similarly for ϕ_{23} and ϕ_{31} between resonators 2 and 3, and 3 and 1, respectively. This difference in the time delay is due to the flow. In the case where two coupled resonators are located on a line perpendicular to

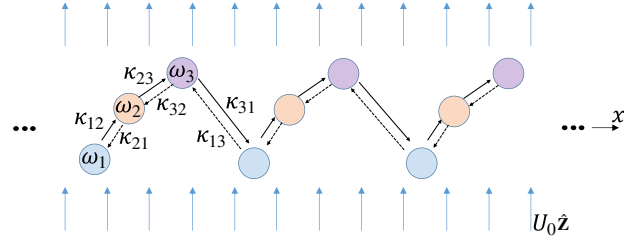


FIG. 10. Kinematic coupled resonator model.

the flow, then the phase will be zero—namely, there will be no difference in the time delay for propagation from resonator 1 to 2, and vice versa. As opposed to that, if the coupled resonators are located in line with the flow, the difference in the time delays will be maximized, and therefore so will the phase. Now, the coupled mode equations that govern the lattice dynamics can be readily formulated as

$$\omega a_n^{(1)} = \omega_1 a_n^{(1)} + \kappa_{21} a_n^{(2)} + \kappa_{31} a_{n-1}^{(3)}, \quad (34a)$$

$$\omega a_n^{(2)} = \kappa_{12} a_n^{(1)} + \omega_2 a_n^{(2)} + \kappa_{32} a_n^{(3)}, \quad (34b)$$

$$\omega a_n^{(3)} = \kappa_{13} a_{n+1}^{(1)} + \kappa_{23} a_n^{(2)} + \omega_3 a_n^{(3)}, \quad (34c)$$

where $a_n^{(i)}$ is the mode amplitude on scatterer number n on chain number i and ω_i is the resonance frequency of the scatterers on chain number i . Because of the structural periodicity, we anticipate a Bloch-form solution. That is, $a_n^{(i)} = a_0^{(i)} e^{-jn\varphi}$, where n is the unit-cell index, i is the chain index, and φ is the phase that is accumulated during the propagation along the lattice. By substituting the Bloch solution into system (34), a homogeneous system for the mode amplitudes $a_0^{(i)}$ is obtained:

$$\begin{pmatrix} \omega_1 - \omega & \kappa_{21} & \kappa_{31} e^{j\varphi} \\ \kappa_{12} & \omega_2 - \omega & \kappa_{32} \\ \kappa_{13} e^{-j\varphi} & \kappa_{23} & \omega_3 - \omega \end{pmatrix} \begin{pmatrix} a_0^{(1)} \\ a_0^{(2)} \\ a_0^{(3)} \end{pmatrix} = 0. \quad (35)$$

The dispersion relation $\varphi(\omega)$ for the modes that are supported by such a lattice is found by setting the homogeneous system determinant to zero, which guarantees non-trivial solutions. This immediately yields the dispersion relation

$$\begin{aligned} & (\omega_1 - \omega)(\omega_2 - \omega)(\omega_3 - \omega) \\ & - [|\kappa_{32}|^2(\omega_1 - \omega) + |\kappa_{13}|^2(\omega_2 - \omega) + |\kappa_{21}|^2(\omega_3 - \omega)] \\ & + 2|\kappa_{12}||\kappa_{23}||\kappa_{31}|\cos(\varphi + \phi_{12} + \phi_{23} + \phi_{31}) = 0. \end{aligned} \quad (36)$$

In the absence of flow, $\phi_{12} = \phi_{23} = \phi_{31} = 0$, and, hence, in light of the evenness of the $\cos(\varphi)$ function, if φ solves

the equation, so does $-\varphi$ and hence the dispersion is symmetric, as expected by a reciprocal guiding structure. Now, in the presence of flow the phase terms are not zero anymore. This will yield a shift in the dispersion diagram. However,

1. even in this case—at any frequency, where a real solution φ_1 can be found—there is necessarily also another real solution φ_2 with opposite group velocity; thus, no one-way guiding band can be predicted by the kinematic model;

2. since the phase terms are proportional to the time-delay difference for propagation between two adjacent resonators, the phase terms that correspond to coupling along the flow or against the flow have opposite signs. This implies that in the presence of transverse flow

$$\phi_{12} + \phi_{23} + \phi_{31} \approx 0. \quad (37)$$

This implies that, using kinematic arguments, a system under transverse flow is practically reciprocal.

In a complete contrast with this intuitive behavior, we showed in the sections above that not only may such a system be strongly nonreciprocal, it may also exhibit a one-way guiding. This is a direct consequence of taking into account not only the time delays but also the actual field distributions. Then, as we show in the main text, only under an interplay between a simultaneous structural gliding asymmetry and the transverse flow, when taking into account the complete field form, is this unique phenomenon obtained. Finally, the kinematic model we provide here can be easily augmented to any number of parallel chains, and, moreover, to any order of “hopping” between the resonators. Using this model, the main result, under transverse flow, will always be the same due to Eq. (37). Namely, practically, no nonreciprocity is predicted in the case of transverse flow using the intuitive kinematic arguments. Therefore, the results in this paper stand as a counterexample against the intuitive picture that was adopted in the Introduction, namely, that acoustic nonreciprocity is caused by momentum bias that imparts from the flow to the acoustic wave. Instead, the physics may get more complex.

V. CONCLUSIONS

We have theoretically shown that a sub-wavelength-thick acoustic waveguide can yield substantial nonreciprocity and even one-way guiding when it is surrounded by mean flow at low Mach numbers, transverse to the waveguide axis. This effect is demonstrated for point-source scatterers in uniform flow, as well as for general monopole and dipole scatterers placed between two media with transverse mean flow velocity. This counterintuitive

phenomenon stems from the interplay between the structural transverse gliding asymmetry and the transverse nonreciprocal interaction between the scatterers that comprise the waveguide. In that sense this phenomenon may be regarded as the acoustic analog to one-way optical waveguiding that is based on the Voigt magneto-optical configuration such as in Ref. [35]. The proposed phenomenon may be used to implement compact, strongly nonreciprocal one-way waveguides for a variety of applications in acoustics, such as for full-duplex communication, energy harvesting, and liquid flow sensing, just to name a few. Lastly, due to the similarity between the physical mechanisms, we expect that our proposed concept for one-way waveguides may also be extended to systems with transverse *synthetic motion* along the waveguide cross section (e.g., by space-time modulation), and thereby also to other physical realms such as electromagnetics and optics.

ACKNOWLEDGMENTS

This research is supported by the Israel Science Foundation (Grant No. 1353/19). Y.H. would like to thank Professor Eldad Avital for insightful discussions.

APPENDIX A: GREEN'S FUNCTION IN A HOMOGENEOUS MEDIUM WITH UNIFORM FLOW

Here we derive closed-form expressions for the elements of the dyadic Green's function that is defined in Eq. (6), for the case of point sources in a homogeneous medium with uniform laminar flow.

Denote by G^{mm} the Green's function that connects a monopole source of volume V to the acoustic pressure P measured at the observer. The pressure derivatives in x and z due to a monopole source will obviously be given via the Green's function:

$$G_x^{md} = \partial_x G^{mm}, \quad G_z^{md} = \partial_z G^{mm}. \quad (A1)$$

Next, since a dipole source with moment D_x or D_z can be considered as the limiting of two adjacent monopoles with opposite monopole volume, then obviously the pressure caused by such a monopole source can be expressed as the negative derivative of the Green's function G^{mm} according to the source coordinates. However, the derivative according to the source coordinate can be replaced by a derivative according to the observer [36]. Therefore,

$$G_x^{dm} = -G_x^{md}, \quad G_z^{dm} = -G_z^{md}. \quad (A2)$$

The remaining four terms are the x and z derivatives of the pressure due to x and z polarized dipoles. Then, it reads

$$G_{xx}^{dd} = \partial_x G_x^{dm}, \quad G_{zz}^{dd} = \partial_z G_z^{dm}, \quad G_{xz}^{dd} = G_{zx}^{dd} = \partial_z G_x^{dm}. \quad (A3)$$

In a medium with uniform flow with velocity $\mathbf{U}_0 = U_0 \hat{\mathbf{z}}$, the pressure Green's function for a monopole source V located at the origin and for an observer located on $y = 0$ reads

$$G^{mm}(\mathbf{r}) = -\frac{\omega^2 \rho_0}{4\pi} \left[\frac{1}{q^2 r} - \frac{q_0 z}{q^2 r^2} + \frac{j q_0 z}{k r^3} \right] e^{jk(q_0 z - r)/q^2}, \quad (\text{A4})$$

where $\mathbf{r} = (x, 0, z)$. Here we have assumed that the monopole is located at the origin and $y = 0$ and $r = \sqrt{q^2 x^2 + z^2}$; k is the wave number in free space ($k = \omega/c_0$); $q^2 = 1 - q_0^2$, where q_0 is the flow's Mach number, $q_0 = U_0/c_0$; and ρ_0 is the medium density.

Below are complete analytical expressions for all Green's functions, for both media, limited to the case where both the source and the observer are located on the $y = 0$ plane. In the expressions below $r = \sqrt{q^2 x^2 + z^2}$. Expressions up to the second-order derivative are presented. In a medium with uniform flow

$$G_x^{md} = -\frac{\omega^2 \rho_0 x}{4\pi} \left[-\frac{jk}{q^2 r^2} - \frac{1}{r^3} + \frac{jk q_0 z}{q^2 r^3} + \frac{3 q_0 z}{r^4} - \frac{3 j q^2 q_0 z}{k r^5} \right] \times e^{jk(q_0 z - r)/q^2}, \quad (\text{A5})$$

$$G_z^{md} = -\frac{\omega^2 \rho_0}{4\pi q^2} \left[\frac{jk q_0}{q^2 r} - \frac{q_0}{r^2} - \frac{jk(1 + q_0^2)z}{q^2 r^2} - \frac{(1 + q_0^2)z}{r^3} + \frac{jk q_0 z^2}{q^2 r^3} + \frac{j q_0 q^2}{k r^3} + \frac{3 q_0 z^2}{r^4} - \frac{3 j q_0 q^2 z^2}{k r^5} \right] \times e^{jk(q_0 z - r)/q^2}. \quad (\text{A6})$$

APPENDIX B: RADIATION CORRECTION FOR AN ACOUSTIC SCATTERER IN A HOMOGENEOUS MEDIUM WITH UNIFORM FLOW

For a passive and lossless scatterer, the power used by an external field to excite the scatterer should be equal to the power radiated by the scatterer:

$$P_{\text{ext}} = P_{\text{rad}}. \quad (\text{B1})$$

To find the radiated power, we perform integration of Poynting's vector PU^* on a cylindrical surface of radius ρ , which stretches from $z = -\infty$ to ∞ :

$$P_{\text{rad}} = \frac{1}{2} \text{Re} \left[\int_{z=-\infty}^{\infty} \int_{\phi=0}^{2\pi} PU_{\rho} d\phi dz \right]. \quad (\text{B2})$$

Given the velocity potential of a monopole scatterer in a uniform medium with mean flow [see Eq. (4)], the velocity

of the medium particles is given by

$$\mathbf{U} = -\nabla \Psi_m. \quad (\text{B3})$$

For an integration on an infinite cylinder, nonzero power flux is only obtained from the radial component of Poynting's vector, which corresponds to the radial velocity $U_{\rho} = -(\partial \Psi_m / \partial \rho)$. Thus, the radial component of Poynting's vector for a monopole in mean flow reads

$$PU_{\rho}^* = \frac{\omega^3 \rho_0 \rho}{16\pi^2} \left[\frac{1}{q^2 r} - \frac{q_0 z}{q^2 r^2} + \frac{j q_0 z}{k r^3} \right] \left[\frac{k}{r^2} + \frac{q^2 j}{r^3} \right] |V|^2, \quad (\text{B4})$$

where $k = \omega/c_0$ is the wave number in stationary medium. This expression should be integrated according to Eq. (B2). We exclude the pressure terms that are odd in z as well as the terms that result with imaginary power and obtain

$$P_{\text{rad}}^m = |V|^2 \frac{1}{2} \text{Re} \int_{z=-\infty}^{\infty} \frac{\omega^3 \rho_0 \rho^2}{8\pi} \frac{k}{q^2 r^3} dz, \quad (\text{B5})$$

which results in

$$P_{\text{rad}}^m = \frac{\omega^3 k \rho_0}{8\pi q^4} |V|^2. \quad (\text{B6})$$

Upon excitation by an external pressure field P_0 , the power the field applies on the particle is $P_{\text{ext}} = -P_0 \dot{V}$. For a time-harmonic external field, the averaged power is

$$P_{\text{ext}}^m = -\frac{\omega}{2} \text{Im}(V^* P_0). \quad (\text{B7})$$

For a passive particle, $P_{\text{ext}} = P_{\text{rad}}$. The monopole susceptibility is defined as $V = \alpha^{mm} P_0$. Comparing Eqs. (B6) and (B7) we get the radiation correction for α^{mm} :

$$\text{Im} \left(\frac{1}{\alpha_{mm}} \right) = -\frac{\omega^3 \rho_0}{4\pi q^4 c_0}. \quad (\text{B8})$$

For a z -polarized dipole in mean flow, the radial component of Poynting's vector reads

$$PU_{\rho}^* = \frac{\omega^3 \rho_0 \rho}{16\pi^2 q^2} \left[\frac{jk q_0}{q^2 r} - \frac{q_0}{r^2} - \frac{jk(1 + q_0^2)z}{q^2 r^2} - \frac{(1 + q_0^2)z}{r^3} + \frac{jk q_0 z^2}{q^2 r^3} + \frac{j q_0 q^2}{k r^3} + \frac{3 q_0 z^2}{r^4} - \frac{3 j q_0 q^2 z^2}{k r^5} \right] \times \left[-\frac{jk^2 q_0}{q^2 r^2} + \frac{jk^2 z}{q^2 r^3} + \frac{k q_0}{r^3} - \frac{3 k z}{r^4} - \frac{3 j q^2 z}{r^5} \right] |D_z|^2. \quad (\text{B9})$$

Losing imaginary and z -odd components yields

$$P_{\text{rad}}^d = \frac{|D_z|^2}{2} \text{Re} \int_{z=-\infty}^{\infty} \frac{\omega^3 \rho_0 \rho^2}{8\pi} \left[\frac{q_0^2 k^3}{q^6 r^3} + \frac{k^3 (1 + 2q_0^2) z^2}{q^6 r^5} \right] dz. \quad (\text{B10})$$

Integration gives

$$P_{\text{rad}}^d = \frac{\omega^3 k^3 \rho_0}{24\pi q^8} (1 + 5q_0^2) |D_z|^2. \quad (\text{B11})$$

As the dipole is basically two monopoles, its excitation power can be written as the sum of excitation powers for both monopoles:

$$P_{\text{ext}}^d = \frac{1}{2} \text{Re}(-P_1 \dot{V}_1^* - P_2 \dot{V}_2^*).$$

The monopoles are at a distance $2l$ from each other and have a phase difference of π , so the expressions for pressure and dipole strength are

$$P_1 = P_0(z + l), \quad \dot{V}_1^* = \dot{V}(r), \quad (\text{B12})$$

$$P_2 = P_0(z - l), \quad \dot{V}_2^* = -\dot{V}(r). \quad (\text{B13})$$

Substituting these relations into the above equation for P_{ext}^d yields

$$\begin{aligned} P_{\text{ext}}^d &= \frac{1}{2} \text{Re}(-P_0(z + l) \dot{V}^* + P_0(z - l) \dot{V}^*) \\ &= -\frac{1}{2} \text{Re} \left(\frac{P_0(z + l) - P_0(z - l)}{2l} 2l \dot{V}^* \right) \\ &= -\frac{\omega}{2} \text{Im} \left(\frac{\partial P_0}{\partial z} D_z^* \right), \end{aligned} \quad (\text{B14})$$

where the dipole moment D_z is defined as $D_z = 2lV$, and in the last equality we took the limit $l \rightarrow 0$. Using $D_z = \alpha_z^{dd} \partial P_0 / \partial z$ and comparing Eqs. (B14) and (B11), we obtain

$$\text{Im} \left(\frac{1}{\alpha_z^{dd}} \right) = -\frac{\omega^5 \rho_0}{12\pi q^8 c_0^3} (1 + 5q_0^2). \quad (\text{B15})$$

For an x -polarized dipole in mean flow, the radial component of Poynting's vector reads

$$\begin{aligned} PU_{\rho}^* &= \frac{\omega^3 \rho_0 x}{16\pi^2} \rho \cos^2(\phi) \\ &\times \left[-\frac{jk}{q^2 r^2} - \frac{1}{r^3} + \frac{jkq_0 z}{q^2 r^3} + \frac{3q_0 z}{r^4} - \frac{3jq^2 q_0 z}{kr^5} \right] \\ &\times \left[\frac{k}{r^2} + \frac{j(q^2 + k^2 \rho^2)}{r^3} - \frac{3kq^2 \rho^2}{r^4} - \frac{3jkq^2 \rho^2}{r^5} \right]. \end{aligned} \quad (\text{B16})$$

Losing imaginary and z -odd components yields

$$P_{\text{rad}} = |D_x|^2 \frac{1}{2} \text{Re} \int_{z=-\infty}^{\infty} \frac{\omega^3 \rho_0 k^3 \rho^4}{16\pi q^2 r^5} dz. \quad (\text{B17})$$

Integration gives

$$P_{\text{rad}}^d = \frac{\omega^3 k^3 \rho_0}{24\pi q^6} |D_x|^2. \quad (\text{B18})$$

Using the exact same process as for the z -polarized dipole and defining $D_x = \alpha_x^{dd} \partial P_0 / \partial x$, we obtain

$$\text{Im} \left(\frac{1}{\alpha_x^{dd}} \right) = -\frac{\omega^5 \rho_0}{12\pi q^6 c_0^3}. \quad (\text{B19})$$

APPENDIX C: CALCULATION OF THE DIAGONAL ELEMENTS (S^{ii}) of \underline{S} —UNIFORM FLOW

Here we calculate the terms of \underline{S} that together with the susceptibility matrix $\underline{\alpha}$ govern the dynamics of the waveguide, according to the dispersion relation in Eq. (15). Here we address the case where the medium is homogeneous, with mean flow $\mathbf{U}_0 = U_0 \hat{z}$, that is, calculating the series in Eqs. (12) and (13), using Green's functions derived in Appendix A. Calculations are based on the methods presented in Ref. [37].

The matrix \underline{S} expresses the local fields in the waveguide, calculated at scatterer 0 in each chain. We start with the diagonal elements of the matrix—element S^{ii} expresses the contribution of the elements in chain i to the local field at scatterer 0 of chain i . If chain i is composed of monopoles,

$$S^{ii} = \sum_{n \neq 0} G^{mm}(nd, 0) e^{-j\beta nd}. \quad (\text{C1})$$

Henceforth, we adopt the notation of a single scatterer's Green's function, where the first and second superscripts of S will denote the exciting and excited scatterers, respectively. Thus, in this case we have $S^{ii} = S^{mm}$. Using Eq. (A4) with $r = q|nd|$, $z = 0$ yields

$$S^{mm} = \sum_{n \neq 0} -\frac{\omega^2 \rho_0}{4\pi q^3 |nd|} e^{-jk|nd|/q} e^{-j\beta nd}. \quad (\text{C2})$$

Separating the series into two, we obtain

$$S^{mm} = -\frac{\omega^2 \rho_0}{4\pi q^3 d} \left[\sum_{n=1}^{\infty} \frac{1}{n} e^{-j(k/q+\beta)nd} + \sum_{n=1}^{\infty} \frac{1}{n} e^{-j(k/q-\beta)nd} \right], \quad (\text{C3})$$

$$S^{mm} = -\frac{\omega^2 \rho_0}{4\pi q^3 d} \left[\text{Li}_1[e^{-j(k/q+\beta)d}] + \text{Li}_1[e^{-j(k/q-\beta)d}] \right], \quad (\text{C4})$$

where Li_1 is polylogarithm of order 1.

For a z -polarized dipole, we define

$$\tilde{L}i_m = Li_m[e^{-j(k/q+\beta)d}] + Li_m[e^{-j(k/q-\beta)d}]. \quad (C5)$$

In the exact same manner as for the monopole, and using G_z^{dd} on the x axis, we obtain

$$S_{zz}^{dd} = -\frac{k^2 q_0^2}{4\pi q^7 d} \tilde{L}i_1 - \frac{jk(1+2q_0^2)}{4\pi q^6 d^2} \tilde{L}i_2 - \frac{1+2q_0^2}{4\pi q^5 d^3} \tilde{L}i_3; \quad (C6)$$

for an x -polarized dipole, we have

$$S_{xx}^{dd} = -\frac{k^2}{4\pi q^5 d} \tilde{L}i_1 + \frac{2jk}{4\pi q^4 d^2} \tilde{L}i_2 + \frac{2}{4\pi q^3 d^3} \tilde{L}i_3. \quad (C7)$$

APPENDIX D: CALCULATION OF THE OFF-DIAGONAL ELEMENTS (S^{Ψ}) OF \underline{S} —UNIFORM FLOW

The off-diagonal elements in \underline{S} represent the effect of one chain on the other. Throughout this section, d_z will denote the distance between chains and d_x will denote the chain gliding. The velocity potential contributed by a chain monopole scatterers at (d_x, d_z) reads

$$S^{\Psi} = \sum_{n=-\infty}^{\infty} e^{-j\beta nd} G^{\Psi}(d_x - nd, d_z), \quad (D1)$$

which is expressed explicitly as

$$S^{\Psi} = \sum_{n=-\infty}^{\infty} j\omega \frac{e^{-j\beta r \sqrt{q^2(d_x - nd)^2 + d_z^2}}}{4\pi \sqrt{q^2(d_x - nd)^2 + d_z^2}} e^{j\beta_z d_z} e^{-j\beta nd}. \quad (D2)$$

Letting $x' = d_x - nd$,

$$S^{\Psi} = \frac{j\omega}{4\pi} e^{j(\beta_z d_z - \beta d_x)} \sum_{n=-\infty}^{\infty} \frac{e^{-j\beta r \sqrt{q^2 x'^2 + d_z^2}}}{\sqrt{q^2 x'^2 + d_z^2}} e^{j\beta x'}. \quad (D3)$$

Expression (D3) converges slowly. A better analytical representation is obtained via Poisson summation, using the formula

$$\sum_{n=-\infty}^{\infty} f(x') = \frac{1}{d} \sum_{n=-\infty}^{\infty} e^{-j2\pi nd_x/d} \int_{-\infty}^{\infty} f(x') e^{j2\pi nx'/d} dx'. \quad (D4)$$

Using the integral result

$$\begin{aligned} & \int_{-\infty}^{\infty} \frac{e^{-j\beta r \sqrt{q^2 x'^2 + d_z^2}}}{\sqrt{q^2 x'^2 + d_z^2}} e^{j(\beta + 2\pi n/d)x'} dx' \\ &= \frac{\pi}{qj} H_0^{(2)} \left[\beta_r d_z \sqrt{1 - \left(\frac{\beta}{\beta_r q} + \frac{2\pi n}{\beta_r q d} \right)^2} \right], \end{aligned} \quad (D5)$$

we define

$$\beta_n = \beta + \frac{2\pi n}{d}, \quad (D6a)$$

$$k_n = \beta_r \sqrt{1 - \left(\frac{\beta_n}{q\beta_r} \right)^2}, \quad (D6b)$$

$$F_n = \frac{\pi}{qj} H_0^{(2)}[k_n d_z], \quad (D6c)$$

and the velocity potential Green's function reads

$$S^{\Psi} = \frac{j\omega}{4\pi d} e^{j\beta_z d_z} \sum_{n=-\infty}^{\infty} e^{-j\beta_n d_x} F_n. \quad (D7)$$

The sign of the square root should be selected based on the physical solution, i.e., as $n \rightarrow \infty$, the argument $k_n d_z$ (which is pure imaginary) should tend to $-\infty$. The pressure Green's function is derived from the velocity potential by Eq. (5); thus, S^{mm} can be written as

$$S^{mm} = j\omega\rho_0 S^{\Psi} + U_0\rho_0 \frac{\partial S^{\Psi}}{\partial d_z}. \quad (D8)$$

The derivative of S^{Ψ} reads

$$\frac{\partial S^{\Psi}}{\partial d_z} = \sum_{n=-\infty}^{\infty} \frac{\partial}{\partial d_z} [F_n(d_z) e^{j\beta_z d_z}]. \quad (D9)$$

We define the derivative of F_n as

$$\frac{\partial F_n}{\partial d_z} = F_{n1}, \quad (D10)$$

$$F_{n1} = -\frac{\pi}{qj} k_n H_1^{(2)}[k_n d_z], \quad (D11)$$

and so

$$\frac{\partial}{\partial d_z} [F_n(d_z) e^{j\beta_z d_z}] = F_{n1} + j\beta_z F_n. \quad (D12)$$

So S^{mm} reads

$$\begin{aligned} S^{mm} &= j\omega\rho_0 \left[\frac{j\omega}{4\pi d} e^{j\beta_z d_z} \sum_{n=-\infty}^{\infty} e^{-j\beta_n d_x} F_n \right] \\ &+ U_0\rho_0 \left[\frac{j\omega}{4\pi d} e^{j\beta_z d_z} \sum_{n=-\infty}^{\infty} e^{-j\beta_n d_x} (F_{n1} + j\beta_z F_n) \right], \end{aligned} \quad (D13)$$

and, after some rearrangement,

$$S^{mm} = -\frac{\omega^2 \rho_0}{4\pi d} e^{j\beta_z d_z} \sum_{n=-\infty}^{\infty} e^{-j\beta_n d_x} \left[\frac{1}{q^2} F_n - \frac{j q_0}{k} F_{n1} \right]. \quad (D14)$$

To obtain $\partial P/\partial z$ generated by the monopole, we have to differentiate S^{mm} , following the same process as above:

$$S_z^{md} = \frac{\partial S^{mm}}{\partial d_z}. \quad (\text{D15})$$

The second derivative of F_n is

$$\frac{\partial^2 F_n}{\partial d_z^2} = F_{n2}, \quad (\text{D16})$$

$$F_{n2} = -\frac{\pi}{qj} \left[k_n^2 H_0^{(2)}[k_n d_z] - \frac{k_n}{|d_z|} H_1^{(2)}[k_n d_z] \right], \quad (\text{D17})$$

$$\frac{\partial^2 F_n}{\partial d_z^2} [F_n(d_z) e^{j\beta_z d_z}] = F_{n2} + 2j\beta_z F_{n1} - \beta_z^2 F_n. \quad (\text{D18})$$

Substituting these relations into Eq. (D15) and rearranging

$$S_z^{md} = -\frac{\omega^2 \rho_0}{4\pi d} e^{j\beta_z d_z} \sum_{n=-\infty}^{\infty} e^{-j\beta_n d_x} \times \left[-\frac{jkq_0}{q^4} F_n - \frac{1+q_0^2}{q^2} F_{n1} + \frac{jq_0}{k} F_{n2} \right]. \quad (\text{D19})$$

The n th summand on the Poisson summation is a Fourier transform of $f(x')$ at frequency β_n ; therefore, we can utilize the Fourier transform property of differentiation on S^{mm} and obtain

$$S_x^{md} = -\frac{\omega^2 \rho_0}{4\pi d} e^{j\beta_z d_z} \sum_{n=-\infty}^{\infty} e^{-j\beta_n d_x} (-j\beta_n) \left[\frac{1}{q^2} F_n - \frac{jq_0}{k} F_{n1} \right]. \quad (\text{D20})$$

Repeating the exact same process as was done to calculate S_z^{md} , we define

$$\frac{\partial^3 F_n}{\partial d_z^3} = F_{n3}, \quad (\text{D21})$$

$$F_{n3} = \frac{\pi}{qj} \left[k_n^3 H_1^{(2)}[k_n d_z] - \frac{k_n^2}{|d_z|} H_2^{(2)}[k_n d_z] \right], \quad (\text{D22})$$

$$\frac{\partial^3 F_n}{\partial d_z^3} [F_n(d_z) e^{j\beta_z d_z}] = F_{n3} + 3j\beta_z F_{n2} - 3\beta_z^2 F_{n1} - j\beta_z^3 F_n, \quad (\text{D23})$$

obtaining, for S_{zz}^{dd} ,

$$S_{zz}^{dd} = -\frac{\omega^2 \rho_0}{4\pi d} e^{j\beta_z d_z} \sum_{n=-\infty}^{\infty} e^{-j\beta_n d_x} \left[-\frac{k^2 q_0^2}{q^6} F_n - \frac{jk(2q_0 + q_0^3)}{q^4} F_{n1} - \frac{1+2q_0^2}{q^2} F_{n2} + \frac{jq_0}{k} F_{n3} \right]. \quad (\text{D24})$$

Differentiating with respect to x' multiplies each summand of S_z^{dm} by $-j\beta_n$, resulting in

$$S_{zx}^{dd} = -\frac{\omega^2 \rho_0}{4\pi d} e^{j\beta_z d_z} \sum_{n=-\infty}^{\infty} e^{-j\beta_n d_x} (-j\beta_n) \times \left[\frac{jkq_0}{q^4} F_n + \frac{1+q_0^2}{q^2} F_{n1} - \frac{jq_0}{k} F_{n2} \right]. \quad (\text{D25})$$

Differentiating S_x^{dm} with respect to x' gives

$$S_{xx}^{dd} = -\frac{\omega^2 \rho_0}{4\pi d} e^{j\beta_z d_z} \sum_{n=-\infty}^{\infty} e^{-j\beta_n d_x} \beta_n^2 \left[\frac{1}{q^2} F_n - \frac{jq_0}{k} F_{n1} \right]. \quad (\text{D26})$$

Lastly, from the relationships in Eqs. (A2) and (A3),

$$S_z^{dm} = -S_z^{md}, \quad S_x^{dm} = -S_x^{md}, \quad S_{xz}^{dd} = S_{zx}^{dd}. \quad (\text{D27})$$

APPENDIX E: SYMMETRY CONDITIONS

Here we outline the circumstances under which the waveguide is nonreciprocal. In a reciprocal waveguide, β and $-\beta$ both solve or do not solve Eq. (15), so for a frequency for which β solves the dispersion relation but $-\beta$ does not, the waveguide will be nonreciprocal.

1. Quiescent medium

In a uniform, quiescent medium ($q_0 = 0$), symmetry relations apply between the scatterer's Green's functions. Denoting by $\underline{\underline{G}}^d$ the dyadic Green's function from Eq. (6) we have

$$\underline{\underline{G}}^d(-x, -z) = \underline{\underline{G}}^d(x, z)^T. \quad (\text{E1})$$

While the diagonal terms of $\underline{\underline{S}}$ do not change, under these relations, $\underline{\underline{S}}$ shows symmetry with respect to β . For example, for two monopole chains,

$$\begin{aligned} S_{ij}(\beta) &= \sum_{n=-\infty}^{\infty} G^{mm}(x = d_x - nd, z = d_z) e^{-j\beta nd} \\ &= \sum_{n=-\infty}^{\infty} G^{mm}(x = d_x + nd, z = d_z) e^{j\beta nd} \\ &= \sum_{n=-\infty}^{\infty} G^{mm}(x = -d_x - nd, z = -d_z) e^{j\beta nd} \\ &= S_{ji}(-\beta). \end{aligned} \quad (\text{E2})$$

This applies to every waveguide geometry and every selection of sources, which implies that $\underline{\underline{S}}(-\beta) = \underline{\underline{S}}^T(\beta)$, and therefore $|\underline{\underline{\alpha}}^{-1} - \underline{\underline{S}}(\beta)| = |\underline{\underline{\alpha}}^{-1} - \underline{\underline{S}}(-\beta)|$.

2. Glided waveguide

For any chain configuration, the self-terms of $\underline{\underline{S}}$ are symmetric with respect to β , so nonreciprocity can stem only from the off-diagonal terms. If $d_x^{ij} = 0$ or $d_x^{ij} = d/2$, S^{ij} may be symmetric or antisymmetric. For S^{mm} , S_z^{md} , S_z^{dm} , S_z^{dd} , S_{xz}^{dd} , we have $S^{ij}(\beta) = S^{ij}(-\beta)$, whereas for S_x^{md} , S_x^{dm} , S_x^{dd} , S_{xz}^{dd} , we have $S^{ij}(\beta) = -S^{ij}(-\beta)$.

If we have N chains of monopoles and transverse dipoles, for every q_0 , $\underline{\underline{S}}$ is symmetric, i.e., $\underline{\underline{S}}(-\beta) = \underline{\underline{S}}(\beta)$, and the determinant is obviously symmetric. If we replace chain i with a chain of longitudinal dipoles, the cross terms of the chain with monopoles or transverse dipoles will all be antisymmetric. Mathematically, this means that the elements in the i th row and i th column of $\underline{\underline{S}}(-\beta)$ are the negatives of the same elements in $\underline{\underline{S}}(\beta)$ (except S^{ii}). In this case $\underline{\underline{S}}(-\beta) \neq \underline{\underline{S}}(\beta)$; however, $|\underline{\underline{\alpha}}^{-1} - \underline{\underline{S}}(\beta)| = |\underline{\underline{\alpha}}^{-1} - \underline{\underline{S}}(-\beta)|$. For example, for a waveguide with three chains and no gliding, consisting of only monopoles and transverse dipoles,

$$\underline{\underline{S}}(\beta) = \underline{\underline{S}}(-\beta) = \begin{bmatrix} S^{11}(\beta) & S^{12}(\beta) & S^{13}(\beta) \\ S^{21}(\beta) & S^{22}(\beta) & S^{23}(\beta) \\ S^{31}(\beta) & S^{32}(\beta) & S^{33}(\beta) \end{bmatrix}.$$

So obviously $|\underline{\underline{\alpha}}^{-1} - \underline{\underline{S}}(\beta)| = |\underline{\underline{\alpha}}^{-1} - \underline{\underline{S}}(-\beta)|$.

By replacing row 2, for example, by a row of longitudinal dipoles we affect elements S^{12} , S^{21} , S^{22} , S^{23} , S^{32} . Now we get

$$\underline{\underline{S}}(-\beta) = \begin{bmatrix} S^{11}(\beta) & -S^{12}(\beta) & S^{13}(\beta) \\ -S^{21}(\beta) & S^{22}(\beta) & -S^{23}(\beta) \\ S^{31}(\beta) & -S^{32}(\beta) & S^{33}(\beta) \end{bmatrix}.$$

Even though the matrices are different, $|\underline{\underline{\alpha}}^{-1} - \underline{\underline{S}}(\beta)| = |\underline{\underline{\alpha}}^{-1} - \underline{\underline{S}}(-\beta)|$. This means that, under these conditions, if β is a solution, so is $-\beta$. These properties are only violated when *at least one* of the chains is shifted to create transverse asymmetry, i.e., with $d_x^{ij} \neq 0, d/2$.

APPENDIX F: CALCULATION OF THE TERMS IN S FOR A STATIONARY MEDIUM BETWEEN TWO HALF-SPACES WITH UNIFORM FLOW—DIRECT WAVES

Here we perform the same process as in Appendices C and D, that is, calculating the terms of the matrix $\underline{\underline{S}}$, while Green's functions are those of a stationary medium between two half-spaces with uniform flow. The direct wave contribution is the contribution of the waves traveling directly from other scatterers, without any reflections. The expressions here are similar to those derived in

Appendices C and D, with $q^2 = 1$:

$$S^{mm} = -\frac{\omega^2 \rho_0}{4\pi d} \left[\text{Li}_1[e^{-j(k+\beta)d}] + \text{Li}_1[e^{-j(k-\beta)d}] \right], \quad (\text{F1})$$

$$S_{zz}^{dd} = -\frac{k^2}{4\pi d} \tilde{\text{Li}}_1 - \frac{jk}{4\pi d^2} \tilde{\text{Li}}_2 - \frac{1}{4\pi d^3} \tilde{\text{Li}}_3, \quad (\text{F2})$$

$$S_{xx}^{dd} = -\frac{k^2}{4\pi d} \tilde{\text{Li}}_1 + \frac{2jk}{4\pi d^2} \tilde{\text{Li}}_2 + \frac{2}{4\pi d^3} \tilde{\text{Li}}_3. \quad (\text{F3})$$

For the off-diagonal elements, we define

$$\beta_n = \beta + \frac{2\pi n}{d}, \quad (\text{F4a})$$

$$k_n = \sqrt{k^2 - \beta_n^2}, \quad (\text{F4b})$$

$$F_n = -j\pi H_0^{(2)}[k_n d_z], \quad (\text{F4c})$$

$$F_{n1} = j\pi k_n H_1^{(2)}[k_n d_z], \quad (\text{F4d})$$

$$F_{n2} = j\pi \left[k_n^2 H_0^{(2)}[k_n d_z] - \frac{k_n}{|d_z|} H_1^{(2)}[k_n d_z] \right]. \quad (\text{F4e})$$

We have

$$S^{mm} = -\frac{\omega^2 \rho_0}{4\pi d} \sum_{n=-\infty}^{\infty} e^{-j\beta_n d_x} F_n, \quad (\text{F5})$$

$$S_z^{md} = -S_z^{dm} = -\frac{\omega^2 \rho_0}{4\pi d} \sum_{n=-\infty}^{\infty} e^{-j\beta_n d_x} F_{n1}, \quad (\text{F6})$$

$$S_x^{md} = -S_x^{dm} = -\frac{\omega^2 \rho_0}{4\pi d} \sum_{n=-\infty}^{\infty} (-j\beta_n) e^{-j\beta_n d_x} F_n. \quad (\text{F7})$$

For dipole-dipole interactions, we have

$$S_{zz}^{dd} = \frac{\omega^2 \rho_0}{4\pi d} \sum_{n=-\infty}^{\infty} e^{-j\beta_n d_x} F_{n2}, \quad (\text{F8})$$

$$S_{zx}^{dd} = S_{xz}^{dd} = -\frac{\omega^2 \rho_0}{4\pi d} \sum_{n=-\infty}^{\infty} (-j\beta_n) e^{-j\beta_n d_x} F_{n1}, \quad (\text{F9})$$

$$S_{xx}^{dd} = -\frac{\omega^2 \rho_0}{4\pi d} \sum_{n=-\infty}^{\infty} e^{-j\beta_n d_x} \beta_n^2 F_n. \quad (\text{F10})$$

APPENDIX G: CALCULATION OF THE TERMS IN S FOR A STATIONARY MEDIUM BETWEEN TWO HALF-SPACES WITH UNIFORM FLOW—REFLECTED WAVES

Here we derive the contribution of the reflected waves only. In this case, the contribution of the particle itself is not excluded, and hence the summation here is performed

according to

$$S_r^{ij}(\beta) = \sum_{n=-\infty}^{\infty} G_r^{ij}(x = d_x^{ij} - nd, z = d_z^{ij}) e^{-j\beta nd}. \quad (\text{G1})$$

This is true for the diagonal terms of $\underline{\underline{S}}$ as well as the off-diagonal terms. We start with the case where both the exciting and excited scatterers are monopoles, meaning that we need to calculate the local reflected pressure at particle X_0^i , contributed by chain i of monopoles:

$$\begin{aligned} P_r(x = d_x^{ij}, z = d_z^{ij}) \\ = \sum_{n=-\infty}^{\infty} G_r^{mm}(x = d_x^{ij} - nd, z = d_z^{ij}) X_0^i e^{-j\beta nd}. \end{aligned} \quad (\text{G2})$$

Thus, we define

$$S_r^{ij}(\beta) = \sum_{n=-\infty}^{\infty} G_r^{mm}(x = d_x^{ij} - nd, z = d_z^{ij}) e^{-j\beta nd}. \quad (\text{G3})$$

From here on we define, for simplicity, $d_x^{ij} = d_x$, $d_z^{ij} = d_z$. Also, we replace the notation S_r^{ij} with S_r^{mm} , to give a general expression for S_r when both chains are composed of monopoles. Thus, the full expression of S_r^{mm} is

$$\begin{aligned} S_r^{mm}(\beta) = \sum_{n=-\infty}^{\infty} \frac{j\omega^2 \rho_0}{8\pi^2} \iint_{-\infty}^{\infty} g_r^{mm}(k_x, k_z) e^{-j(k_x(d_x - nd) + k_z d_z)} \\ \times e^{-j\beta nd} dk_x dk_z, \end{aligned} \quad (\text{G4})$$

where g_r^{mm} is the spectrum of the reflected field,

$$g_r^{mm}(k_x, k_z) = \frac{2\text{Re}^{-jk_y L}}{k_y(1 - \text{Re}^{-jk_y L})}. \quad (\text{G5})$$

Inverting the order of summation and integration yields

$$\begin{aligned} S_r^{mm}(\beta) = \frac{j\omega^2 \rho_0}{8\pi^2} \iint_{-\infty}^{\infty} g_r^{mm}(k_x, k_z) e^{-j(k_x d_x + k_z d_z)} \\ \times \sum_{n=-\infty}^{\infty} e^{j(k_x - \beta)nd} dk_x dk_z. \end{aligned} \quad (\text{G6})$$

We use the identity

$$\sum_{n=-\infty}^{\infty} e^{j(k_x - \beta)nd} = \sum_{n=-\infty}^{\infty} \frac{2\pi}{d} \delta(k_x - \beta_n), \quad (\text{G7})$$

where $\beta_n = \beta + 2\pi n/d$. After using the identity and integrating dk_x we get

$$S_r^{mm}(\beta) = \frac{j\omega^2 \rho_0}{4\pi d} \sum_{n=-\infty}^{\infty} \int_{-\infty}^{\infty} g_r^{mm}(\beta_n, k_z) e^{-j(\beta_n d_x + k_z d_z)} dk_z. \quad (\text{G8})$$

The relationships between Green's functions in Eqs. (A1)–(A3) apply in this case as well, so we can readily obtain expressions for other exciting and excited scatterers through the differentiation properties of Fourier transform. For example,

$$\begin{aligned} S_{xr}^{md}(\beta) = \frac{j\omega^2 \rho_0}{4\pi d} \sum_{n=-\infty}^{\infty} \int_{-\infty}^{\infty} -j\beta_n g_r^{mm}(\beta_n, k_z) \\ \times e^{-j(\beta_n d_x + k_z d_z)} dk_z, \end{aligned} \quad (\text{G9})$$

$$\begin{aligned} S_{zr}^{md}(\beta) = \frac{j\omega^2 \rho_0}{4\pi d} \sum_{n=-\infty}^{\infty} \int_{-\infty}^{\infty} -jk_z g_r^{mm}(\beta_n, k_z) \\ \times e^{-j(\beta_n d_x + k_z d_z)} dk_z. \end{aligned} \quad (\text{G10})$$

The fact that the chain is infinite allows us to calculate the elements of $\underline{\underline{S}}$ using one-dimensional integration instead of two-dimensional integration. For β_n with $|n| > 0$, the integrand decays very rapidly, so summing only a few elements is enough to get accurate results.

APPENDIX H: FINITE CHAIN SOLUTION—NUMERICAL ASPECTS

When solving a finite excitation problem for a waveguide in a stationary medium between two flowing half-spaces, we need to solve system (17), where the elements of matrix $\underline{\underline{G}}$ read

$$G[k, l] = \begin{cases} G_{\text{FS}}^{ij}(\mathbf{r}^k - \mathbf{r}^l) + G_r^{ij}(\mathbf{r}^k - \mathbf{r}^l), & k \neq l, \\ G_r^{ij}(\mathbf{r}^k - \mathbf{r}^l), & k = l. \end{cases} \quad (\text{H1})$$

Here, \mathbf{r}^k and \mathbf{r}^l are the locations of scatterers $\mathbf{X}[k]$ and $\mathbf{X}[l]$, and i, j are the chain numbers of scatterers k, l , respectively. While G_{FS}^{ij} has an analytical expression and is easy to calculate, G_r^{ij} should be calculated numerically according to the integral in Eq. (32). This numerical integration is hard to perform with accuracy for two reasons:

1. g_r^{ij} has pole singularities where $\text{Re}^{-jk_y L} = 1$;
2. as per Eq. (32), for large values of x , the integrand becomes very oscillatory.

The second reason is what makes simulation of long chains harder. To integrate more accurately, we use complex integration. In Eq. (32), we change the integration path dk_ρ from the interval $[0, \infty]$ to a path over the curve:

$$k_\rho = k \left(\xi + j \frac{2\Delta}{\pi} \arctan \xi \right) \quad (\text{H2})$$

with $\xi : 0 \rightarrow \infty$. Following this curve avoids the singularity on the real axis; the smaller $|\Delta|$ is, the closer the curve

is to the singular point. However, if $|\Delta|$ is too large, the integrand will turn very large. Therefore, a gentle selection of Δ should be made, as well as a very fine spectral discretization. The results presented here are obtained using brute-force integration, and are verified for accuracy and stability. Another approach would be the replacement of the original integration path by integration around singular points in the complex plane, i.e., poles, and branch cuts. Since we seek an exact solution, the integration complexity around the branch cuts will remain similar to what we currently have. Therefore, it does not suggest a significant improvement. For asymptotic evaluation though, it will be superior. Other expedite numerical recipes for Green's function calculations may also be applicable here [38–42], but since it is not the heart of this work, we decided to use a more expensive albeit brute-force approach.

-
- [1] R. Fleury, D. Sounas, M. Haberman, and A. Alú, Nonreciprocal acoustics, *Acoust. Today* **11**, 14 (2015).
- [2] H. Nassar, B. Yousefzadeh, R. Fleury, M Ruzzene, A. Alú, C. Daraio, A. N. Norris, G. Huang, and M. R. Haberman, Nonreciprocity in acoustic and elastic materials, *Nat. Rev. Mater.* **5**, 667 (2020).
- [3] B. Liang, B. Yuan, and J. C. Cheng, Acoustic Diode: Rectification of Acoustic Energy Flux in One-Dimensional Systems, *Phys. Rev. Lett.* **103**, 104301 (2009).
- [4] N. Boechler, G. Theocharis, and C. Daraio, Bifurcation-based acoustic switching and rectification, *Nat. Mat.* **10**, 665 (2011).
- [5] J. Cui, T. Yang, and L. Q. Chen, Frequency-preserved non-reciprocal acoustic propagation in a granular chain, *Appl. Phys. Lett.* **112**, 181904 (2018).
- [6] B. I. Popa and S. A. Cummer, Non-reciprocal and highly nonlinear active acoustic metamaterials, *Nat. Commun.* **5**, 3398 (2014).
- [7] X. Guo, H. Lissek, and R. Fleury, Improving Sound Absorption Through Nonlinear Active Electroacoustic Resonators, *Phys. Rev. Appl.* **13**, 014018 (2020).
- [8] Y. Zhai, H. S. Kwon, and B. I. Popa, Active Willis metamaterials for ultra-compact non-reciprocal linear acoustic devices, *Phys. Rev. B* **99**, 220301(R) (2019).
- [9] O. Godin, Reciprocity and energy theorems for waves in a compressible inhomogeneous moving fluid, *Wave Motion* **25**, 143 (1997).
- [10] C. P. Wiederhold, D. L. Sounas, and A. Alú, Nonreciprocal acoustic propagation and leaky-wave radiation in a waveguide with flow, *J. Acoust. Soc. Am.* **146**, 802 (2019).
- [11] P. Wang, L. Lu, and K. Bertoldi, Topological Phononic Crystals with One-Way Elastic Edge Waves, *Phys. Rev. Lett.* **115**, 104302 (2015).
- [12] Philip M. Morse and K. Uno Ingrad, *Theoretical Acoustics* (McGraw-Hill, New York NY, 1968).
- [13] R. Fleury, D. Sounas, C. Sieck, M. Haberman, and A. Alú, Sound isolation and giant linear nonreciprocity in a compact acoustic circulator, *Science* **343**, 516 (2014).
- [14] Y. Ding, Y. Peng, Y. Zhu, X. Fan, J. Yang, B. Lang, X. Zhu, X. Wan, and J. Cheng, Experimental Demonstration of Acoustic Chern Insulators, *Phys. Rev. Lett.* **122**, 014302 (2019).
- [15] Z. Yang, X. Shi, X. Lin, Z. Gao, Y. Chong, and B. Zhang, Topological Acoustics, *Phys. Rev. Lett.* **114**, 114301 (2015).
- [16] R. Fleury, D. Sounas, and A. Alú, Subwavelength ultrasonic circulator based on spatiotemporal modulation, *Phys. Rev. B* **91**, 174306 (2015).
- [17] N. Jankovic and A. Alú, Glide-Symmetric Acoustic Waveguides for Extreme Sensing and Isolation, *Phys. Rev. Appl.* **15**, 024004 (2021).
- [18] L. Quan, D. Sounas, and A. Alú, Nonreciprocal Willis Coupling in Zero-Index Moving Media, *Phys. Rev. Lett.* **123**, 064301 (2019).
- [19] Y. Wang, B. Yousefzadeh, H. Chen, H. Nassar, G. Huang, and C. Daraio, Observation of Nonreciprocal Wave Propagation in a Dynamic Phononic Lattice, *Phys. Rev. Lett.* **121**, 194301 (2018).
- [20] C. Croënne, J. O. Vasseur, O. Bou Matar, A.-C. Hladky-Hennion, and B. Dubus, Non-reciprocal behavior of one-dimensional piezoelectric structures with space-time modulated electrical boundary conditions, *J. Appl. Phys.* **126**, 145108 (2019).
- [21] J. Huang and X. Zhou, A time-varying mass metamaterial for non-reciprocal wave propagation, *Int. J. Sol. Struct.* **164**, 25 (2019).
- [22] H. Nassar, X. C. Xu, A. N. Norris, and G. I. Huang, Modulated phononic crystals: Non-reciprocal wave propagation and Willis materials, *J. Mech. Phys. Solids* **101**, 10 (2017).
- [23] N. Swintek, S. Matsuo, K. Runge, J. O. Vasseur, P. Lucas, and P. A. Deymier, Bulk elastic waves with unidirectional backscattering-immune topological states in a time-dependent superlattice, *J. Appl. Phys.* **118**, 063103 (2015).
- [24] R. Fleury, A. B. Khanikaev, and A. Alú, Floquet topological insulators for sound, *Nat. Commun.* **7**, 11744 (2016).
- [25] To see this, we write the wave equation for the pressure field in a fluid with uniform mean flow velocity $U_0\hat{z}$: $(\partial_t + U_0\partial_z)^2 p = c^2 \nabla^2 p$. Considering propagation only in the x - z plane, its monochromatic plane-wave solution is $p(x, z, t) = p_0 e^{-j(k_x x + k_z z)} e^{j\omega t}$, and subject to the dispersion relation $k_z^2 + k_x^2 = k^2 - 2kU_0k_z/c + U_0^2k_z^2/c^2$. Clearly, for a plane wave that propagates parallel to the x axis (z axis), $k_z = 0$ ($k_x = 0$), and therefore $k_x = \pm k$ [$k_z = k/(q_0 \pm 1)$], where $k = \omega/c$ is the wavenumber in the stationary medium and q_0 is the Mach number. Then, the phase velocity reads $v_p = \omega/k_{x,z}$, and thus $\tau_d^{A \leftrightarrow B} = L/v_p$.
- [26] The condition for the existence of propagating modes in the waveguide is $d < \lambda/2$ when the medium is quiescent ($U_0 = 0$). However, when a uniform transverse flow is added, the condition is slightly different, requiring $d < \sqrt{1 - q_0^2} \lambda/2$, where q_0 is the flow's Mach number.
- [27] L. Quan, Y. Ra'di, D. L. Sounas, and A. Alú, Maximum Willis Coupling in Acoustic Scatterers, *Phys. Rev. Lett.* **120**, 254301 (2018).
- [28] M. Quinten, A. Leitner, J. R. Krenn, and F. R. Aussenegg, Electromagnetic energy transport via linear chains of silver nanoparticles, *Opt. Lett.* **23**, 1331 (1998).

- [29] A. Alú and N. Engheta, Theory of linear chains of meta-material/plasmonic particles as subdiffraction optical nanotransmission lines, *Phys. Rev. B* **74**, 205436 (2006).
- [30] Y. Hadad and B. Z. Steinberg, Magnetized Spiral Chains of Plasmonic Ellipsoids for One-Way Optical Wave Guides, *Phys. Rev. Lett.* **105**, 233904 (2010).
- [31] Y. Hadad and B. Z. Steinberg, Greens function theory for infinite and semi-infinite particle chains, *Phys. Rev. B* **84**, 125402 (2011).
- [32] Y. Hadad, Y. Mazor, and B. Z. Steinberg, Greens function theory for one-way particle chains, *Phys. Rev. B* **87**, 035130 (2013).
- [33] J. W. Miles, On the reflection of sound at an interface of relative motion, *J. Acoust. Soc. Am.* **29**, 226 (1957).
- [34] Hermann A. Haus, *Waves and Fields in Optoelectronics* (Prentice-Hall, Englewood Cliffs, NJ, 1984).
- [35] Y. Mazor, Y. Hadad, and B. Z. Steinberg, Planar one-way guiding in periodic particle arrays with asymmetric unit cell and general group-symmetry considerations, *Phys. Rev. B* **92**, 125129 (2015).
- [36] If the monopole source is expressed by $V\delta(|x - x'|)\delta y\delta(z)$ then a dipole with moment D_x is defined such that the positive monopole is located at $x = x'^+$ while the negative monopole is located at $x = x'^-$. Then, clearly the dipole source is expressed by $-D_x[d\delta(|x - x'|)/dx']\delta(y)\delta(z) = -D_x[d\delta(|x - x'|)/dx]\delta(y)\delta(z)$.
- [37] Y. Mazor, Y. Hadad, and B. Z. Steinberg, Clustering in particle chains—summation techniques for the periodic Green's function, ArXiv (2017).
- [38] G. Dural and M. I. Aksun, Closed-form Green's functions for general sources and stratified media, *IEEE Trans. Microw. Theory Tech.* **43**, 1545 (1995).
- [39] M. I. Aksun, A robust approach for the derivation of closed-form Green's functions, *IEEE Trans. Microw. Theory Tech.* **44**, 651 (1996).
- [40] V. I. Okhmatovski and A. C. Cangellaris, A new technique for the derivation of closed-form electromagnetic Green's functions for unbounded planar layered media, *IEEE Trans. Antennas Propag.* **50**, 1005 (2002).
- [41] V. I. Okhmatovski and A. C. Cangellaris, Evaluation of layered media Green's functions via rational function fitting, *IEEE Microw. Wireless Compon. Lett.* **14**, 22 (2004).
- [42] Y. Hadad, On the use of the Padé-Fourier approximation in fast evaluation of the Green's function of layered media, Preprint ArXiv:2111.09089 (2022).